Preclinical Evaluation of 9MW2821, a Site-Specific Monomethyl Auristatin E–based Antibody–Drug Conjugate for Treatment of Nectin-4–expressing Cancers

Wei Zhou[1,2,3], Peng Fang[2,4], Dongan Yu[2,4], Hongyuan Ren[2], Meng You[2,4], Long Yin[2,4], Fei Mei[2,4], Huikai Zhu[2], Zhenzhen Wang[2], Hui Xu[2], Yuxia Cao[2,4], Xiaowei Sun[2,4], Xiaohong Xu[2], Jianjun Bi[2], Jin Wang[2], Lanping Ma[3], Xin Wang[3], Lin Chen[3], Yongliang Zhang[3], Xiaowei Cen[2], Xi Zhu[3], Liguang Lou[3], Datao Liu[2], Xiaoding Tan[2], Jinliang Yang[1], Tao Meng[3], and Jingkang Shen[3]

ABSTRACT

Overexpression of nectin cell adhesion protein 4 correlates with cancer progression and poor prognosis in many human malignancies. Enfortumab vedotin (EV) is the first nectin-4–targeting antibody–drug conjugate (ADC) approved by the FDA for the treatment of urothelial cancer. However, inadequate efficacy has limited progress in the treatment of other solid tumors with EV. Furthermore, ocular, pulmonary, and hematologic toxic side effects are common in nectin-4–targeted therapy, which frequently results in dose reduction and/or treatment termination. Thus, we designed a second generation nectin-4–specific drug, 9MW2821, based on interchain-disulfide drug conjugate technology. This novel drug contained a site specifically conjugated humanized antibody and the cytotoxic moiety monomethyl auristatin E. The homogenous drug–antibody ratio and novel linker chemistry of 9MW2821 increased the stability of conjugate in the systemic circulation, enabling highly efficient drug delivery and avoiding off-target toxicity. In preclinical evaluation, 9MW2821 exhibited nectin-4–specific cell binding, efficient internalization, bystander killing, and equivalent or superior antitumor activity compared with EV in both cell line–derived xenograft and patient-derived xenograft (PDX) models. In addition, 9MW2821 demonstrated a favorable safety profile; the highest nonseverely toxic dose in monkey toxicologic studies was 6 mg/kg, with milder adverse events compared with EV. Overall, 9MW2821 is a nectin-4–directed, investigational ADC based on innovative technology that endowed the drug with compelling preclinical antitumor activity and a favorable therapeutic index. The 9MW2821 ADC is being investigated in a phase I/II clinical trial (NCT05216965 and NCT05773937) in patients with advanced solid tumors.

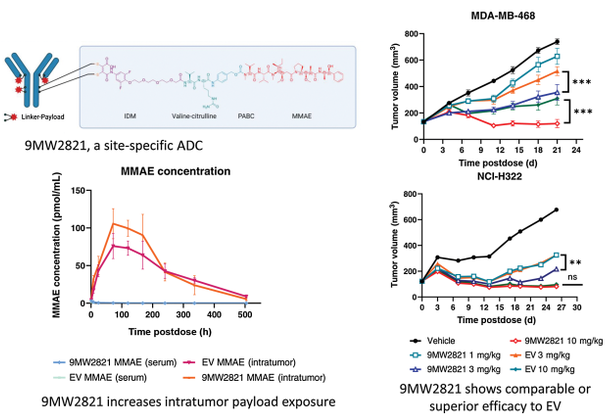

Introduction

Nectin-4 is a member of the nectin family of Ca^{2+}-independent Ig-like adhesion molecules (1, 2). Structurally, nectin family members have three Ig-like extracellular loops and a single transmembrane region. Nectins are important for the formation and maintenance of adherence and tight junctions. Unlike nectin-1, 2, and 3, which are widely expressed in adult tissues, nectin-4 is expressed only in the embryo and placenta (1, 3). Nectin-4 is an epithelial receptor for the measles virus, suggesting that it is a promising target for oncolytic and immune therapy based on recombinant morbilli viruses (4, 5). Overexpression of nectin-4 is also associated with the growth and invasion of various tumors and poor prognosis. Thus, nectin-4 is a reliable serum and tissue cancer biomarker (6–9). Nectin-4 activates the WNT-β–catenin pathway and the small G protein Rac in the PI3K-AKT signaling pathway (10–13). Nectin-4 also interacts with the tyrosine kinase receptor ERBB2, which results in stimulation of the PI3K-AKT pathway (14). Under hypoxic conditions, the soluble parts of nectin-4 enhance angiogenesis by interacting with endothelial integrin-β4, an essential component of the metastatic pathway (2, 15). Furthermore, nectin-4 acts as a novel T-cell Ig and ITIM domain (TIGIT) ligand that can specifically bind TIGIT without influencing

[1]Department of Biotherapy, Cancer Center and State Key Laboratory of Biotherapy/Collaborative Innovation Center for Biotherapy, West China Hospital, Sichuan University, Chengdu, China. [2]Mabwell (Shanghai) Bioscience Co., Ltd., Shanghai, China. [3]Shanghai Institute of Materia Medica, Chinese Academy of Sciences, Shanghai, China. [4]Jiangsu Mabwell Health Pharmaceutical R&D Co., Ltd., Taizhou, China.

Corresponding Authors: Xiaoding Tan, Mabwell (Shanghai) Bioscience Co., Ltd., Shanghai 201203, China. E-mail: xiaoding.tan@mabwell.com; Jinliang Yang, State Key Laboratory of Biotherapy and Cancer Center/Collaborative Innovation Center for Biotherapy, West China Hospital, Sichuan University, Chengdu 610041, China. E-mail: jinliangyang@scu.edu.cn; and Tao Meng, Shanghai Institute of Materia Medica, Chinese Academy of Sciences, 555 Zu Chong Zhi Road, Shanghai 201203, China. E-mail: tmeng@simm.ac.cn

Mol Cancer Ther 2023;22:913–25

doi: 10.1158/1535-7163.MCT-22-0743

CD112R, CD96, or DNMA1. Antibody blocking of the nectin-4 interaction with TIGIT activates the immune system against tumors (16).

Antibody–drug conjugates (ADC) are a promising class of therapies designed to deliver cytotoxic chemotherapy specifically to antigen-expressing tumor cells (17, 18). Treatment efficacy is primarily related to the level of antigen expression (19, 20). Enfortumab vedotin (EV), an anti–nectin-4 ADC, is highly effective against urothelial carcinoma because of the high nectin-4 expression level of this cancer (10, 21). The FDA granted accelerated approval for EV for locally advanced or metastatic urothelial cancer for patients who had previously received a programmed cell death protein 1 (PD-1) or programmed cell death ligand 1 (PD-L1) inhibitor and platinum-containing chemotherapy or who were ineligible for cisplatin-containing chemotherapy (22). However, the outcomes of EV treatment are relatively disappointing for other nectin-4–expressing tumors, and limited clinical efficacy is reported for EV and BT8009 (an anti–nectin-4 peptide–drug conjugate) in clinical trials (23). In addition, ocular, pulmonary, and toxic hematologic side effects were widely associated with these two nectin-4–targeted therapies, which frequently led to discontinuation of treatment (24, 25).

Here, we report development and preclinical evaluation of 9MW2821 (**Fig. 1A**), a novel nectin-4–targeting ADC composed of an anti–nectin-4 antibody (MW282 mAb), a novel linker, IDconnect, and a known cytotoxic moiety, that is, the tubulin polymerization inhibitor monomethyl auristatin E (MMAE). IDconnect is designed to form site-specific disulfide bonds by cross-linking the reduced cysteines in the Fab and hinge regions of an antibody, thereby rendering a highly homogeneous drug-to-antibody ratio of 4 (DAR4). The conjugation process is efficient, high yielding, and generates stable products with minimal unconjugated fragments (Supplementary Fig. S1A and S1B). We evaluated the 9MW2821 conjugate for its antigen specificity, internalization process, cytotoxicity, bystander killing effect, pharmacokinetics, biodistribution, antitumor efficacy, and safety profile. The results from these preclinical studies suggested that 9MW2821 had the desired characteristics of an antitumor agent that warrants further clinical development for treatment of multiple cancers.

Materials and Methods

Generation of parental antibody for 9MW2821

The parental antibody of 9MW2821 was MW282 mAb, produced by Mabwell Health, Inc. The final sequence of MW282 mAb was acquired by mouse immunization, hybridoma screening, humanization, and affinity maturation (26). The posttranslational modification sites were replaced by similar nonmodifiable amino acids or by previously tested residues (27). The sequences that code light-chain and heavy-chain of MW282 mAb were cloned in an expression vector that was transfected into CHO K1 cells, followed by monoclonal cell line selection and generation of three sublevels of cell bank (primary cell bank, master cell bank, and working cell bank) for mAb production. The cell lines were thawed from the working cell bank and stepwise amplified in flasks in a wave25 bioreactor (Cytiva) and XDR200 bioreactor. We used fed-batch mode to culture the cells in Dynamis (Gibco) medium supplemented with Cell Boost 7a (HyClone), Cell Boost 7b (HyClone), and glucose (Sigma). Operational parameters for the bioreactor were set as 37°C, pH 7.0±0.2, 40% of dissolved oxygen, and 90 rpm for impeller speed throughout the cultivation. Antifoam (Sigma) was used to foam control during cultivation. Cell culture bulk was harvested by deep filtration (Millistak+ HC Pro C0SP, Merck) after 13 to 14 days of cultivation. Antibodies were purified by a classic purification process for therapeutic mAbs that included Protein A affinity chromatography (Cytiva, MabSelected SuRe LX), low pH inactivation, cation exchange chromatography (Cytiva, Capto S ImPact), and anion exchange chromatography (Cytiva, Q Sepharose Fast-Flow), followed by virus nanofiltration (MSPV01FS1 and VPMD103NB1, Millipore). We also strictly controlled the critical quality characteristics of antibodies during production. The purity was measured by size exclusion chromatography (SEC) and denaturing capillary electrophoresis with SDS (denaturing CE-SDS). The exact molecular weight was measured by intact mass analysis. The analytic methods used are listed in the Supplementary Data.

Preparation of ADC

The 9MW2821 was prepared from fully reduced MW282 mAb obtained by using excess tris (2-carboxyethyl) phosphine hydrochloride (8 molar equivalents per mAb). The linker payload was added to the reduced solvent at 5-molar equivalent linker-payload/mAb ratio and incubated for 1 h to produce the ADC intermediate. After hydrolysis in phosphate buffer (pH 8.0), the ADC intermediate was purified by preparative hydrophobic interaction chromatography to obtain 9MW2821 with a fixed DAR4. Throughout the production process, the yield of 9MW2821 was 65% (28). Enfortumab vedotin (EV, Lot#102374), purchased from Astellas, was used as a benchmark ADC.

DAR was measured by hydrophobic interaction chromatography (HIC) and native mass spectrometry. Purity was determined by SEC. Isomeric distribution was determined by CE-SDS (29). The analytic methods used are listed in the Supplementary Data. We also used HIC and CE-SDS to compare the structures of 9MW2821 and EV.

Cell lines

Cell lines NCI-H322, HT1376, BT474, MDA-MB-231, T24, PC-3, and SW780 were purchased from the ATCC; MDA-MB-468 cells were purchased from the National Collection of Authenticated Cell Cultures of the Chinese Academy of Sciences. Cell lines were passaged for no more than 2 months after their resuscitation and maintained at 37 °C with a 5% CO_2 atmosphere in appropriate media. All cell lines were authenticated by short tandem repeat (STR) DNA profiling and tested negative for *Mycoplasma* contamination by the 4′6-diamidino-2-phenylindole DNA fluorescence staining method. Cell lines MDA-MB-231/nectin-4, T24/nectin-4, SW780/nectin-4, and PC-3/nectin-4 were generated by infecting cells with lentivirus vector pLenti-puro that contain the complete human *nectin-4* gene. The lentiviral vector was packaged in HEK-293T cells and used to infect MDA-MB-231, T24, SW780, and PC-3 cells. Positive clones were obtained by screening with 2 μg/mL puromycin, and monoclonal cell lines that stably expressed a high level of nectin-4 were obtained by limiting the dilution method. Blank control cell lines MDA-MB-231/vector, T24/vector, SW780/vector, and PC-3/vector were generated by infecting cells with lentivirus that contained vector alone. We used flow cytometry analysis to measure nectin-4 expression in all cell lines.

ELISA

We used a competitive ELISA to measure the nectin-4–binding affinities of 9MW2821, its parental mAb (MW282 mAb), and EV. The antigen, mammalian cell-expressed recombinant human nectin-4 extracellular domain was coated onto the ELISA plate. After blocking the plate with BSA, the plate was incubated with biotin-labeled MW282 mAb at a fixed concentration mixed with serially diluted

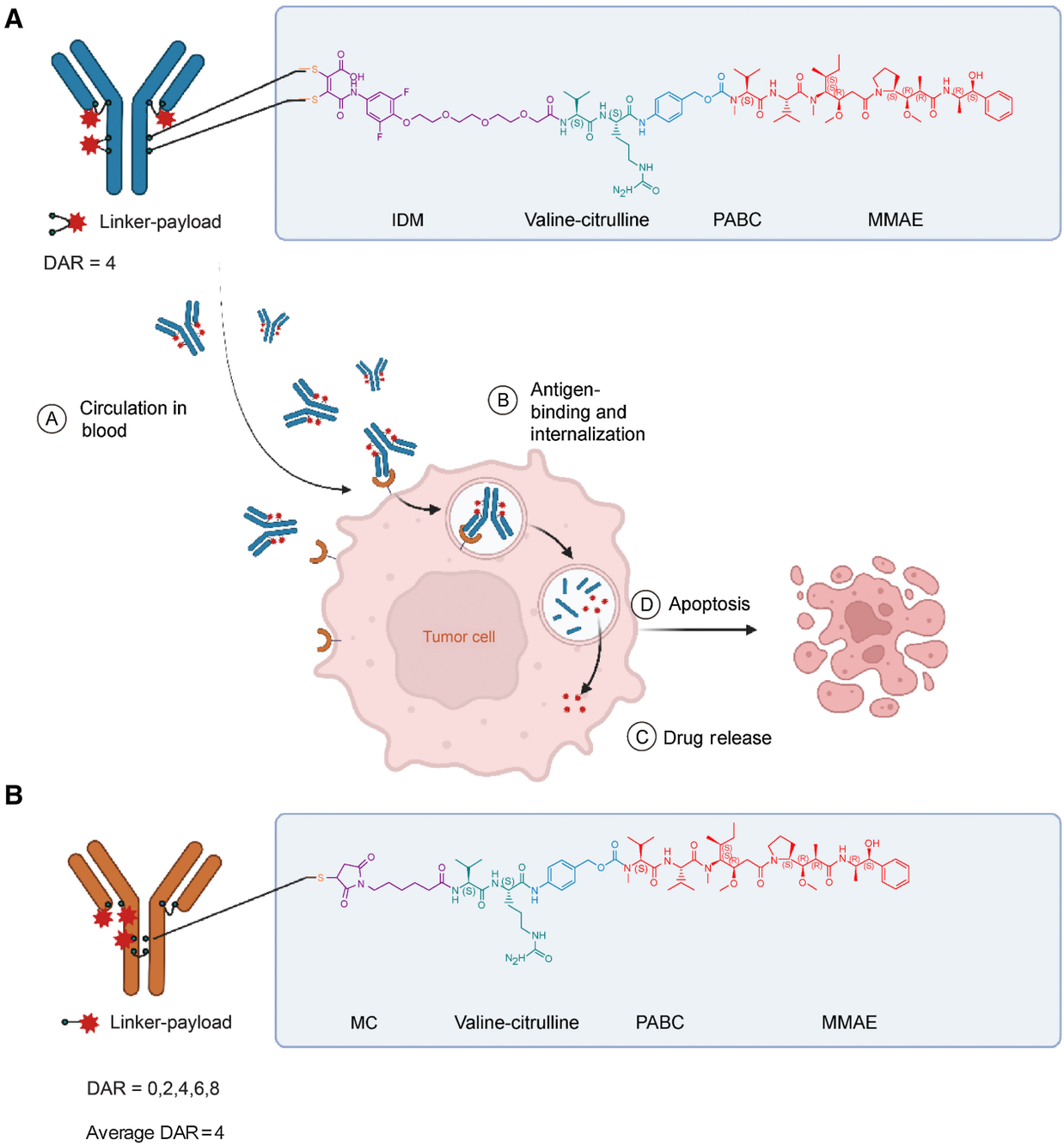

Figure 1.
Structure and characterization of 9MW2821 and EV. **A,** Chemical structure of 9MW2821 contains three key components, a nectin-4 specific antibody, a hydrolyzable di-substituted maleimide (IDM) with a cleavable valine-citrulline dipeptide, and a microtubule inhibitor MMAE. **B,** Chemical structure of EV. Images were created with Biorender.com.

9MW2821, MW282 mAb, or EV. Then the plate was washed and incubated with horseradish peroxidase (HRP)-conjugated streptavidin. Tetramethylbenzidine was used as the chromogenic reagent, and the reaction was terminated with phosphoric acid. Optical density at 450 nm was measured using a multifunction microplate reader (Molecular Devices, SpectraMax M5).

The cross-reactivity of 9MW2821 with nectin family proteins was evaluated by ELISA. Mammalian cell–expressed recombinant human nectin-1, nectin-2, nectin-3, and nectin-4 extracellular domains were diluted to 1 μg/mL and coated on an ELISA plate, followed by washing and blocking with BSA. Then, serial concentrations of 9MW2821 were added to the wells, followed by washing and incubation with

HRP-conjugated goat anti-human secondary antibodies. Finally, tetramethylbenzidine was used as a chromogenic reagent, the reaction was terminated by phosphoric acid, and a multifunction microplate reader was used to measure the optical density at 450 nm.

Bio-Layer Interferometry

Bio-Layer Interferometry technology was used to measure the binding kinetics and activity of ADC toward antigenic protein. Binding kinetics were measured with the Octet RED96 instrument (ForteBio, Pall Corporation). Anti-hIgG Fc Capture (AHC) biosensor tips were utilized to capture 9MW2821, EV, or MW282 monoclonal antibodies (mAb) at a concentration of 100 mmol/L. Subsequently, three samples were incubated with gradually diluted soluble antigenic proteins (nectin-4 from Puremab, #9997-N4–050) ranging from 3.125 to 50 mmol/L to determine the binding kinetics. The obtained data were globally fitted to different binding schemes, corresponding to a 1:1 Langmuir binding isotherm.

Antibody-dependent cell-mediated cytotoxicity

Antibody-dependent cell-mediated cytotoxicity (ADCC) of the MW282 mAb, 9MW2821, and EV was assessed using a cell-based reporter-gene assay. The assay consisted of a genetically engineered Jurkat cell line, acting as the effector cell, which stably expressed the FcgRIIIa receptor. These cells also contained a luciferase expression moiety driven by a nuclear factor of active T cells (NFAT) response element. The PC-3/nectin-4 cell line that expressed human nectin-4 on the cell surface was selected as the target cell line to investigate the ADCC effect. Products with ADCC activity bound to the FcγRIIIa receptor and activated the downstream NFAT signaling pathway, followed by luciferase expression in a dose-dependent manner. The luciferase level was measured with addition of the Bio-Glo Luciferase Assay System (Promega, catalog No. G7940), and the signal was acquired with a microplate reader (Molecular Devices, SpectraMax M5). To confirm the activation of the NFAT signal pathway, the Jurkat cells were harvested when coculture with target cell was completed, in the presence of high (1 μg/mL) or low (20 ng/mL) level of drugs. The phosphorylated NFAT2 (Abcam, catalog No. ab183023) in Jurkat cell was detected by immunoblotting with GAPDH (Cell Signaling Technology, catalog No. 2118S) as control housekeeping gene. The activation of the NFAT signaling pathway in Jurkat cells was indicated by a reduction in the level of phosphorylated NFAT2 (30).

Surface plasmon resonance

The affinities of the antibodies to recombinant human Fcγ and FcRn receptors were determined using Biacore 8 K (GE Healthcare). For human Fcγ and FcRn receptor affinity measurement, 50 μg/mL mouse anti-His tag mAb (GE Healthcare, catalog No. 29234602 and catalog No. 29234600) was covalently immobilized on a carboxymethyl dextran–coated sensor chip CM5 (GE Healthcare, catalog No. BR-1005–30), followed by capturing His-tagged recombinant human FcγRI (CD64), Fcγ RIIA (CD32a), Fcγ RIIb (CD32b), Fcγ RIIIa (CD16a), and FcRn. Serially diluted antibodies were injected into the chip with 30 μL/minute flow rate, and signals were acquired for affinity analysis according to the manufacturer's recommendations.

IHC analysis

We randomly selected 178 formalin-fixed, paraffin-embedded (FFPE) samples, including 46 cervical cancers, 61 breast cancers (including 26 triple-negative breast cancers), 35 lung cancers, 30 gastric cancers, and six prostate cancers, and cut them into 3- to 5-μm-thick slides. IHC was performed using the Leica Bond RX platform. After deparaffinization and rehydration, tissue sections were treated for antigen retrieval with EDTA (pH 9.0) for 20 minutes at 100°C and incubated with 1:100 diluted anti–nectin-4 rabbit polyclonal antibodies (Cell Signaling Technology Inc., catalog No. 17402) or irrelevant rabbit mAb (Abcam Inc., catalog No. ab172730) for 1 h at room temperature. Expression was detected using the Bond Polymer Refine Detection Kit (Leica Inc.), including anti-rabbit poly-HRP-IgG and DAB chromogenic reagents. Stained sections were scanned using a Pannoramic Digital Slide Scanners at 40× magnification (3DHISTECH, Ltd.). High-resolution pictures were generated for all sections. All images were analyzed with the HALO platform (Indica Labs). With reference to the histochemical scoring system (H-score) defined by Challita-Eid and colleagues (21), we multiplied the sum of the products of staining intensity (score of 0–3) by the percentage of cells (0–100) stained at a given intensity. The specimens were classified as negative (H-score 0–14), weak (H-score 15–99), moderate (H-score 100–199), or strong (H-score 200–300). Patient information is shown in Supplementary Tables S1–4.

In vitro cytotoxicity

The cytotoxicities of 9MW2821, MW282 mAb, and MMAE were evaluated with cell lines that expressed different levels of human nectin-4. The cell lines were seeded in 96-well plates. After overnight incubation, the three test articles (9MW2821, MW282 mAb, and MMAE) were separately added to different wells. The concentrations of the two drugs were 0 to 100 μg/mL, and the MMAE payload range was 0.001 nmol/L to 10 nmol/L. After 96-h incubation, cell viability was measured by MTS, and the concentration of ADC that inhibited half maximal cell growth (IC_{50}) was calculated according to a four-parameter fitting curve.

Bystander killing effect

To measure a bystander killing effect of 9MW2821 and EV, PC-3 and PC-3/nectin-4 cell lines were used as nectin-4–negative and positive cells, respectively. For the coculture study, PC-3 cells were seeded in a 6-well plate at fixed 3×10^4 cells/well, and PC-3/nectin-4 cells were seeded at 0, 0.3×10^4, 3×10^4, and 6×10^4 cells/well. After overnight incubation, the supernatant was removed, and each drug, MW282 mAb, 9MW2821, and EV, was added to 1 μg/mL (no added drug was the control). After 5 days of coculture, the supernatant was removed, and viable cells were detached from the plate. The number of cells was measured with a cell counter. To determine the ratio of PC-3 and PC-3/nectin-4 cells, the cells were stained with a mouse monoclonal anti-nectin–4 antibody (Clone# M008, prepared by Mabwell) on ice for 60 minutes. After washing, the cells were stained with goat anti-mouse FITC (Abcam, catalog No. ab150113) on ice for 60 minutes. After washing, the fluorescent signals of 1×10^4 stained cells were measured using a flow cytometer, and the ratio of nectin-4–positive to nectin-4–negative cells was calculated. The number of PC-3 or PC-3/nectin-4 cells in each well was calculated, and the bystander killing effect was evaluated on the basis of the number of PC-3 cells.

Internalization

The internalization of anti-nectin-4 antibodies was evaluated by flow cytometry analysis, and antibody intracellular location was determined by laser scanning confocal microscopy of nectin-4–expressing cells.

For flow cytometry analysis, two typical cell lines (PC-3/nectin-4 for nectin-4 high expression, MDA-MB-468 for nectin-4 medium expression) were used to evaluate the internalization. Cells were seeded in

a 6-well plate with 0.3 to 0.5 million cells/well and cultured with medium containing 1 μg/mL Alexa Fluor 488-labeled MW282 mAb, 9MW2821, or EV for 3, 6, 18, 24, and 48 h at 37 °C. After culturing, the cells were detached and harvested by trypsinization, followed by washing and flow cytometric analysis (CytoFlex).

For the drug intracellular location study, Alexa Fluor 488-labeled 9MW2821 (0.5 μg/mL) was incubated with PC-3/nectin-4 cells for 0.5, 1, 2, 3, or 4 h at 37°C, and lysosomes were stained with a lysosomal red fluorescent probe (LysoTracker Deep Red, Invitrogen) for 15 minutes. After washing twice with warm PBS, the cells were photographed with a laser scanning confocal microscope (Leica TCS SP8).

In vitro serum stability study

To assess serum stability *in vitro*, 9MW2821 and EV were incubated at 37°C for up to 14 days in cynomolgus monkey serum (CDSER, Shanghai Institute of Materia Medica, Shanghai, China). Considering the possible effect of concentration on the results, we measured drug samples at 5,000 ng/mL and 50,000 ng/mL. Total antibodies and intact ADC were quantified by ELISA-based assay. Free MMAE was quantified by LC/MS-MS. The quantification method is shown in Supplementary Data.

Pharmacokinetics and tissue distribution in tumor-bearing mice

To evaluate drug pharmacokinetics and distribution, breast tumor-bearing mice (MDA-MB-468) were administered 9MW2821 and EV at 3 mg/kg. Total antibodies, intact ADC, and free MMAE in mouse serum and tumor tissue were measured at 1, 8, 24, 72, 120, 168, 240, 336, and 504 h after injection. Mouse serum was directly analyzed to measure drug concentrations, and the supernatants of tumor tissue homogenates were used to measure drug concentrations. Total antibodies and intact ADC in serum were quantified by ELISA-based assay. Free MMAE in serum and tumor tissues were quantified by LC/MS-MS. The analytic method was consistent with the method used to measure stability in serum *in vitro* (Supplementary Materials and Methods). Tissue distribution was also studied with ^{89}Zr-labeled ADC in tumor-bearing mice. The 9MW2821 was conjugated with p-SCN-Bn-deferoxamine and labeled with ^{89}Zr, as described previously (31–33). The purity and stability of the labeled samples were qualified by radio-HPLC using column TSKgel G3000SWXL (Tosoh Corporation) and eluted at 0.8 mL/minute in 0.1 mol/L PB+0.2 mol/L NaCl+10% ACN.

MDA-MB-468 tumor-bearing nude mice ($n = 5$) were administered a single intravenous dose of ^{89}Zr-9MW2821 (about 4.9 mg/kg, 67.0 μCi/mouse). PET/CT static scans were performed at 0.08, 24, 48, 72, 120, 168, and 240 h after drug administration. After scanning, image processing and reconstruction were performed with PMOD software (PMOD Technologies LLC). The region of interest was outlined, including the entire brain (no division), heart, liver, spleen, lungs, kidneys, bones and joints, muscles, and tumors. Radioactivity was measured by gamma counting, and radioactivity concentration was expressed as a percentage of the injected dose per gram (%ID/g).

Antitumor efficacy of 9MW2821 in cell line–derived xenograft

The antitumor efficacy of 9MW2821 was evaluated in triple-negative breast cancer (MDA-MB-468), lung cancer (NCI-H322), and urothelial carcinoma (HT1376) xenograft models.

Antitumor efficacy was evaluated using 1, 3, and 10 mg/kg of 9MW2821 via intravenous injection. As a reference compound, EV was included at 3 mg/kg and 10 mg/kg in the three xenograft models. Mice injected with the same volume of saline were used as controls. In three studies, 8 to 10 mice were assigned to each dose group. Before initiating the first dose, all tumors were permitted to grow to 100 to 150 mm^3.

Tumor growth inhibition (TGI) was calculated using the formula TGI (%) = [1 – (T – T0)/ (C – C0)] ×100%, where T and T0 were the tumor volume and initial tumor volume in the drug-treated group, respectively, and C and C0 were the tumor volume and initial tumor volume in the control group. The tumor volume and animal body weight were measured twice per week.

All procedures related to animal handling, care, and treatment in the studies were performed according to the guidelines approved by the Institutional Animal Care and Use Committee (IACUC) of Shanghai Institute of Materia Medica (Shanghai, China), following the guidance of the Association for Assessment and Accreditation of Laboratory Animal Care.

Antitumor efficacy of 9MW2821 in patient-derived xenograft

All *in vivo* procedures were conducted in compliance with the guidelines of the Institutional Animal Care and Use Committee at Mabwell Bioscience or commissioned contract research organization (CRO), which are fully accredited by the Association and Accreditation of Laboratory Animal Care. In all xenograft studies, no weight loss or treatment-related toxicities were observed for mice treated with any of the test articles.

Seven patient-derived xenograft (PDX) models were used to predict the benefit of 9MW2821 as a nectin-4 ADC in different clinical circumstances. Similar to the scheme of the cell line-derived xenograft (CDX) models, six mice were randomly assigned to the treatment or control group, and the first dose was administered when the tumors grew to 100 to 150 mm^3. The dosing regimen was 3 mg/kg once a week (QW) × 3. The drug efficacy toward large tumors was also evaluated. In CV13641, LU3037, and BR3578 xenograft studies, the vehicle-treated group was administered 3 mg/kg QW × 3 when tumor volume reached about 1,100 mm^3.

TGI was calculated using the formula TGI (%) = [1 – (T – T0)/ (C – C0)] × 100%. The tumor volume and animal body weight were measured twice per week.

General toxicology studies

In general toxicology studies, cynomolgus monkeys were used to estimate the safety and toxicokinetic profile of 9MW2821. Fifty cynomolgus monkeys from five groups (five animals/sex/group) received five doses (i.v., QW×5) of vehicle (0 mg/kg), 9MW2821 (1, 3, and 6 mg/kg) or MW282 mAb (6 mg/kg). Thirty animals (three animals/sex/group) were necropsied at the end of the dosing phase (day 31), and the remaining 20 animals (two animals/sex/group) were necropsied at the end of the recovery phase (day 58). Clinical observations were continuously performed for ophthalmology, body weight, food consumption, body temperature, and pathology. Concurrently, the cardiovascular system safety, pharmacology, and assessment of local irritation were monitored.

Toxicokinetic studies were incorporated into the repeated-dose toxicity study. Within the treatment dose range, blood samples were collected in the first and fourth dose cycles for toxicokinetic and immunogenic analyses. The concentrations of 9MW2821 and total antibodies in serum were determined with a validated ligand-binding assay, and the concentrations of MMAE were measured by LC/MS-MS. The quantification method is shown in Supplementary Data.

Statistical analysis

Phoenix WinNonlin 8.1 was used to calculate the pharmacokinetic parameters in the noncompartment model, including t1/2, Tmax,

Cmax, AUC0-t, and AUC0-∞. The *in vitro* data were analyzed and displayed using PRISM 8.0 (GraphPad) software. The half maximal effective concentration (EC_{50}) and half maximal inhibitory concentration (IC_{50}) were calculated using a nonlinear regression model with sigmoidal fitting. The *in vitro* antitumor activities of drugs were evaluated by a two-tailed paired *t* test.

Data availability

Data generated in this study are available within the article and its supplementary data files or from the corresponding author upon reasonable request.

Results

Generation and characterization of 9MW2821

The parental antibody of 9MW2821, MW282 mAb, is a recombinant anti–nectin-4 humanized antibody expressed in Chinese hamster ovary (CHO) cells. We used many methods to ensure the quality of MW282 mAb. Intact mass analysis showed that the molecular weight of MW282 mAb was 146,000 Da, which matched theoretical molecular weight of 145,997 Da. The MW282 mAb also showed acceptable physicochemical properties for subsequent ADC preparation. Size exclusion chromatography and denaturing capillary electrophoresis showed a high purity of MW282 mAb. About 99.5% monomer and 0.5% aggregate was observed in size exclusion chromatography, and 97.5% monomer and 2.5% fragment was observed in denaturing capillary electrophoresis. The analytical results are shown in Supplementary Table S5; Supplementary Fig. S2A–S2C.

The 9MW2821 conjugate was derived by connecting the MW282 mAb with MMAE by an IDconnect and a protease cleavable peptide-based linker (**Fig. 1A**). We attached the IDconnect, a unique maleimide scaffold that was substituted with a 4-mercapto-benzoyl-morpholine group serving as the leaving group at both the 3- and 4-positions. This attachment was achieved by cross-linking the IDconnect to the reduced cysteines located in the Fab and hinge regions of the MW282 monoclonal antibody (mAb) (**Fig. 1A**; Supplementary Fig. S1A and S1B). Complete hydrolysis of the maleimide prevented deconjugation by the retro-Michael reaction.

The 9MW2821 appeared as a homogeneous ADC with a DAR of 4 (>95%; **Fig. 1A**; Supplementary Fig. S2A and S2B); other ADC such as EV display DARs in the range of 1 to 8 (**Fig. 1B**, Supplementary Fig. S3A–S3E). To reduce the hydrophobicity of 9MW2821, we used PEG4 as the spacer in the linker. Intact mass analysis showed that the molecular weight of 9MW2821 was 152,148 Da, consistent with theoretical molecular weight of 152,144 Da for the DAR 4 component. Size exclusion chromatography showed that the purity of 9MW2821 was 98.8%, and aggregation was not observed during the conjugation process. Hydrophobic interaction chromatography (HIC) showed that 9MW2821 contained a major DAR 4 component with 97.6% purity, which was greater than the 42.8% purity of EV. Denaturing capillary electrophoresis revealed only two isomeric products of 9MW2821. We observed peaks that corresponded to LHHL and HL with 98.3% purity, and little unconjugated fragments, such as HH, L, and HHL, were detected. Compared with most reported disulfide bridging methods (34–38), 9MW2821 showed the greatest homogeneity with minimal unconjugated fragments. Detailed analytic results are shown in Supplementary Table S6 and Supplementary Fig. S2–S4.

Binding affinity and specificity

The 9MW2821 conjugate had strong and specific binding to recombinant human nectin-4, with EC_{50} 6.97 ng/mL, and it did not bind to nectin-1, nectin-2, or nectin-3 (Supplementary Fig. S5). Furthermore, a competitive ELISA assay showed that 9MW2821 had an affinity for nectin-4 similar to the nectin-4 affinity of EV, with EC_{50} values of 1,456 ± 37 ng/mL and 1,452 ± 46 ng/mL, respectively ($P > 0.5$). The 9MW2821 conjugate appeared to have greater affinity than its parental antibody MW282 mAb that had an EC_{50} value of 1,296 ± 23 ng/mL ($P < 0.01$). The detailed binding information is shown in Supplementary Table S7 and Supplementary Fig. S6.

We also used Bio-Layer Interferometry to measure the binding kinetics and affinities of 9MW2821, EV, and MW282 mAb for nectin-4. The 9MW2821 conjugate had a higher affinity compared with EV, with a dissociation constant (K_d) of 0.85 ± 0.03 nmol/L versus 3.35 ± 0.05 nmol/L for EV ($P < 0.01$). The k_{on} values of 9MW2821 and EV were numerically similar ($3.75 \pm 0.021^{*}10^{5}$ M^{-1} s^{-1}, $4.17 \pm 0.29^{*}10^{5}$ M^{-1} s^{-1}, $P > 0.05$); however, the K_{off} of 9MW2821 was significantly less than EV ($3.20 \pm 0.085^{*}10^{-4}$ s^{-1}, $14.0 \pm 0.80^{*}10^{-4}$ s^{-1}, $P < 0.01$); this finding indicated a lower dissociation rate of 9MW2821 after binding the antigen and possibly explained the better *in vivo* efficacy of 9MW2821. The detailed Bio Layer interferometry binding information is shown in Supplementary Table S8 and Supplementary Fig. S7.

ADCC and affinity to Fcγ and FcRn

Another important attribute of an ADC is its Fc function, which profoundly affects the bioactivities, immunogenicity, and rate of clearance from circulation. As measured by a cell-based reporter-gene assay, the MW282 mAb, 9MW2821, and EV exhibited relatively high ADCC, with MW282 mAb having the highest ADCC (Supplementary Table S9; Supplementary Fig. S8A and S8B). We confirmed the activation of the NFAT signal pathway in Jurkat cells in the presence of drugs by observing a reduction in the level of phosphorylated NFAT2. We also used surface plasmon resonance to evaluate the affinity of 9MW2821 for Fcγ and FcRn receptors. The affinity of 9MW2821 for Fcγ and FcRn receptors was generally similar to the affinities of MW282 mAb and EV (Supplementary Table S10). All the results for Fc function indicated that both 9MW2821 and EV had a typical IgG1 antibody Fc effect, and the Fc function was not significantly altered after conjugation (Supplementary Fig. S9).

IHC analysis

We used IHC to measure the level of nectin-4 expression in 178 randomly selected tumor samples. The detailed information including cancer type, gender, pathology, gene expression is shown in Supplementary Tables S1–3. In agreement with a report by Challita-Eid and colleagues (21), we observed high nectin-4 expression in various cancers (**Fig. 2A**). Most cancers were nectin-4-positive. Only 10% of the samples exhibited H-scores greater than 200; however, in breast cancer, lung cancer, cervical cancer, and prostate cancer, 30% to 50% of the samples had H-scores greater than 100. If we included an H score of 15 to 100, this population was extended to 70% of the samples.

Nectin-4 expression and *in vitro* cytotoxicity

We used flow cytometry analysis to measure the relative expression of nectin-4 on the cell surface. The nectin-4–overexpressing cell lines constructed by gene engineering, SW780/nectin-4, T24/nectin-4, MDA-MB-231/nectin-4, and PC-3/nectin-4, showed extremely high mean fluorescence intensity (MFI) values, whereas the corresponding nectin-4–null cell lines (SW780/vector, T24/vector, MDA-MB-231/vector, and PC-3/vector) had lower binding to 9MW2821. The native cell lines MDA-MB-468, NCI-H322, and HT1376 showed moderate MFI values. (**Fig. 2C**; Supplementary Table S11).

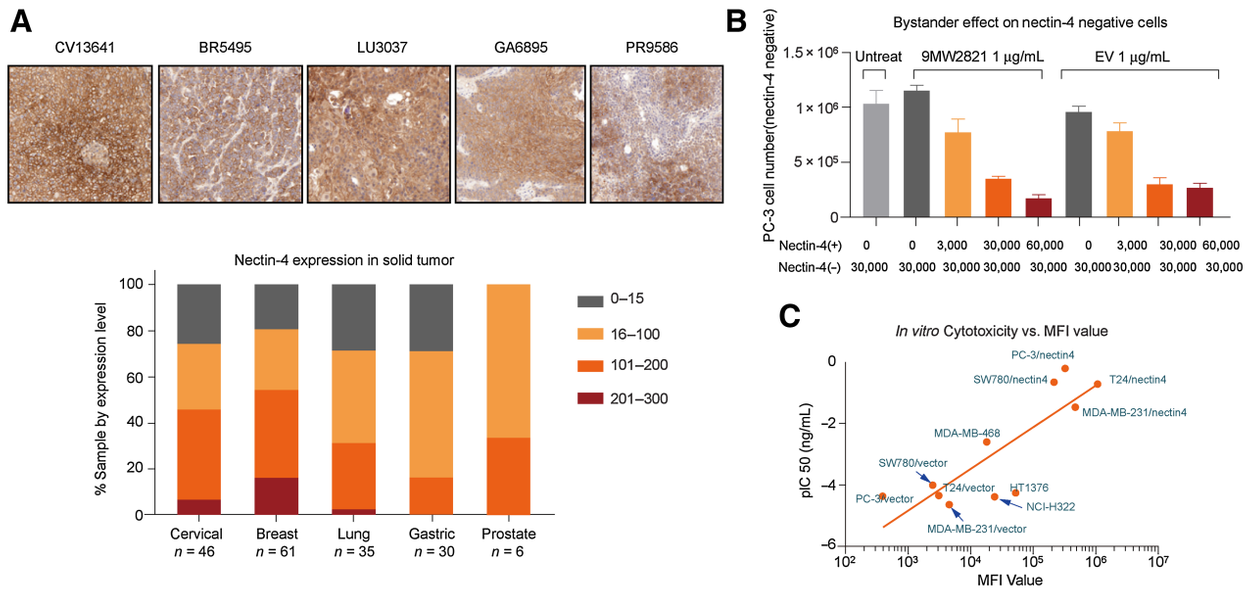

Figure 2.

Antigen expression and *in vitro* cytotoxicity. **A,** FFPE samples (176) were analyzed by IHC for H-score. Most cancers were nectin-4-positive. Although only 10% of the samples exhibited an H-score greater than 200, in breast cancer, lung cancer, cervical cancer, or prostate cancer, 30% to 50% exhibited an H-score greater than 100. **B,** Bystander killing effect of 9MW2821 and EV. Nectin-4–negative PC-3 cells were unaffected by 9MW2821 and EV, whereas the negative PC-3 cells were inhibited when the PC-3/nectin-4 (nectin-4–positive cells) were gradually added. Each experiment was performed three times to calculate the mean cytotoxicity and SD. **C,** The relation between antigen expression and ADC efficacy. The pIC_{50} are mean values of triplicate measurements of each cell line.

The 9MW2821 conjugate exhibited substantial cytotoxicity in cell lines with high nectin-4 expression but was less effective toward medium and low nectin-4–expressing cell lines. The free MMAE displayed potent cytotoxicity toward all cell lines, whereas MW282 mAb showed no inhibitory activities. Thus, the MMAE alone was responsible for inducing cytotoxicity and apoptosis of the tumor cells (**Fig. 2C**; Supplementary Table S11).

Bystander killing effect

The bystander cytotoxicity effect is typically attributed to ADC that release cell-permeable payloads and has been demonstrated for MMAE ADC in several studies (39). The bystander effect may have a positive impact in decreasing tumor stroma and tumor cells with no or less target expression, thereby enhancing the antitumor effectiveness of ADC. To investigate the bystander killing effect of 9MW2821 and EV, we conducted a coculture cell killing assay. PC-3 cells (3×10^4) were mixed with PC-3/nectin-4 cells at ratios from 0 to 6×10^4. In the absence of PC-3/nectin-4 cells, neither 9MW2821 nor EV showed significant growth inhibition of the PC-3 cells. As the number of PC-3/nectin-4 cells was increased, the cell growth inhibition of PC-3 increased. The 9MW2821 and EV conjugates showed similar bystander killing toward the PC-3 cell in the presence of varying numbers of PC-3/nectin-4 cells (**Fig. 2B**).

Internalization

We used laser scanning confocal microscopy to observe internalization and intracellular localization of 9MW2821. The 9MW2821 conjugate exhibited a high endocytic activity. At the beginning of incubation, 9MW2821 was generally located on the cell surface. Subsequently, 9MW2821 gradually became internalized and trafficked to the lysosome in PC-3/nectin-4 cells. After 4 h, 9MW2821 colocalized with the lysosome marker (**Fig. 3A**).

We used flow cytometry analysis to evaluate the kinetics of 9MW2821 internalization with PC-3/nectin-4 (nectin-4 high expression) and MDA-MB-468 (nectin-4 medium expression) cells, which were incubated with fluorescein-labeled MW282 mAb, 9MW2821, and EV for different times. As the incubation time increased, all three entities gradually accumulated in the cells. In terms of the internalization rate, both 9MW2821 and EV showed a similar rate on PC-3/nectin-4 cells with high nectin-4 expression. However, the internalization rate of MW282 mAb was the lowest. For nectin-4 medium–expressing cells, MDA-MB-468, 9MW2821 exhibited more rapid internalization compared with MW282 mAb and EV (**Fig. 3B** and **C**).

In vitro serum stability

To measure the stability of 9MW2821 and EV in serum *in vitro*, we used LC/MS-MS and ELISA to measure the concentrations of free MMAE, total antibodies, and ADC during the course of 14 days in cynomolgus monkey serum. The release rate of free MMAE was relatively low and similar for the two ADC as measured by LC/MS-MS (**Fig. 4A**). However, as measured in an ELISA test, EV degraded more rapidly than 9MW2821. We found that 45.5% of 9MW2821 and 77.7% of EV was degraded in the serum after 14 days (**Fig. 4B**), whereas the total antibodies of the two ADC remained at a high level (**Fig. 4C**). It is known that the maleimide linker can rapidly transfer to albumin, which causes instability of the maleimide (40–42). Spontaneous succinimide ring hydrolysis of 9MW2821 avoided thioether exchange, thereby maintaining DAR and preventing albumin adduct formation.

Pharmacokinetic and tissue distribution of 9MW2821 in tumor-bearing mice

To explain the underlying antitumor effect of 9MW2821, we measured the pharmacokinetics and pharmacodynamics of 9MW2821

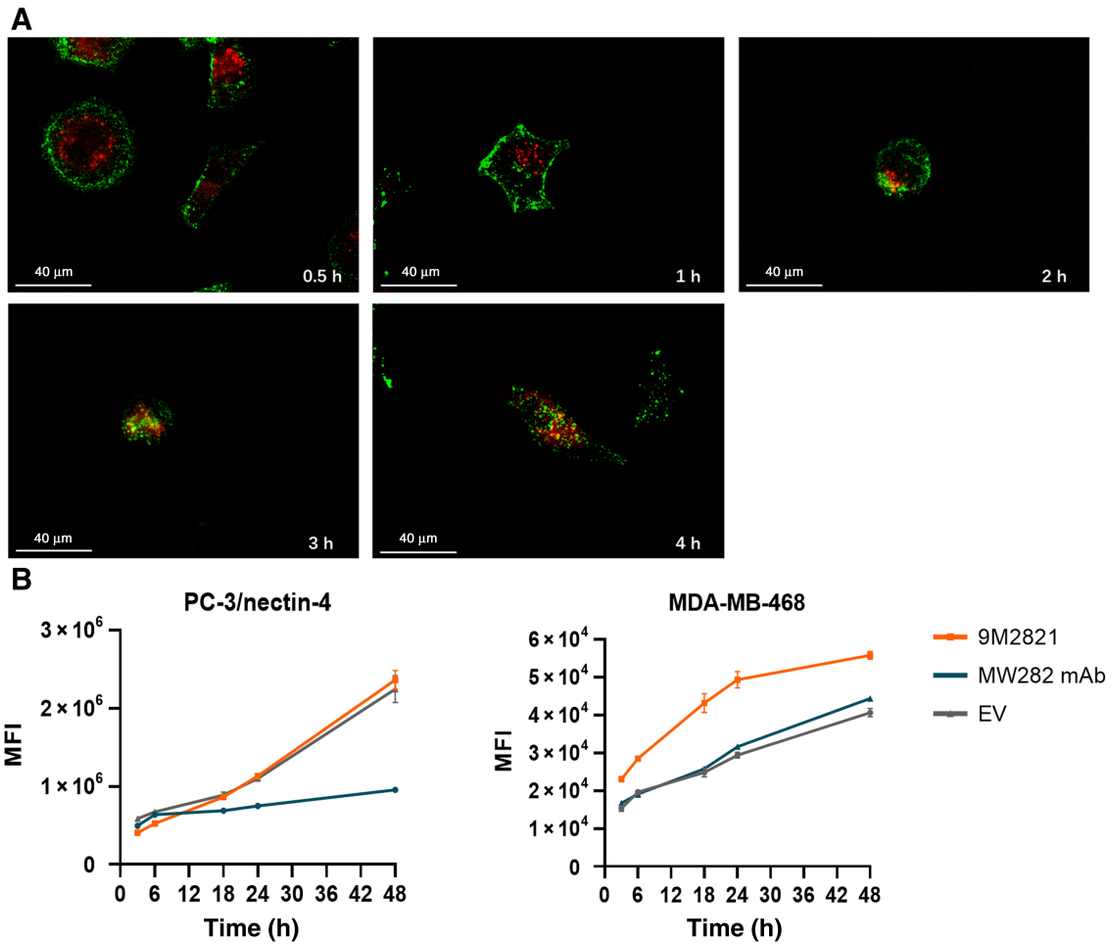

Figure 3.

Internalization and lysosomal trafficking. MW282 mAb, 9MW2821, and EV were labeled with Alexa Fluor 488 using a commercial Alexa Fluor 488 conjugation kit (Abcam, catalog No. ab236553). **A,** Internalization and lysosomal trafficking of 9MW2821 in PC-3/nectin-4 cells, stained for lysosomes (red) and 9MW2821 (green). Costaining of lysosomes and 9MW2821 observed as yellow. Scale bars, 100 μm. **B** and **C,** Fluorescence signal increased as drugs accumulated intracellularly. Alexa Fluor 488–labeled MW282 mAb, 9MW2821, and EV were internalized and stored continuously in PC-3/nectin-4 (left) and MDA-MB-468 (right). Fluorescence signals are mean values of triplicate measurements for each cell line.

and EV in a triple-negative breast cancer MDA-MB-468 subcutaneous xenograft model.

As shown in **Figs. 4D** and **E**, total antibody and 9MW2821 concentrations rapidly reached the C_{max} values (56.5, 52.8 μg/mL) and then gradually decreased, whereas the free MMAE concentrations in circulation were at low levels (0.002 μg/mL). Conversely, the concentrations of 9MW2821 and MMAE in intratumoral cells peaked at 8 h and 72 h, respectively and remained at comparable levels at 168 h and 336 h. The highest concentration of MMAE in tumor tissue was 106 pmol/mL, which was about 38 times greater than that of free MMAE in the blood.

The pharmacokinetic study showed that EV and 9MW2821 were substantially similar in pharmacokinetic profile (**Fig. 4G** and **H**). However, the serum exposure of 9MW2821 was 2,020 h/μg/mL, which was lower than the serum exposure of EV, 2,497 h/μg/mL ($n = 6$, $P < 0.05$). The intratumoral MMAE C_{max} and exposure for 9MW2821 were much higher than those of EV. The C_{max} of 9MW2821 was 106 pmol/mL and EV was 76 pmol/mL ($n = 6$, $P < 0.01$; **Fig. 4F**). The AUC $_{0\text{-t}}$ of intratumor MMAE was 2,452 pmol/mL/h in the 9MW2821 group and 2,116 pmol/mL/h in the EV group ($n = 6$, $P < 0.05$). Detailed pharmacokinetic information is shown in Supplementary Table S12.

An ^{89}Zr-labeled 9MW2821 derivative illustrated another aspect of drug distribution in animals and tumor tissues. The 9MW2821 conjugate was distributed mainly in tumors and organs with rich blood flow, that is, heart, liver, lung, spleen, and kidney (**Fig. 4I** and **J**). Intratumoral drug concentrations remained elevated (radioactive uptake %ID/g > 5) 24 to 240 h after dosing. Simultaneously, the absorption of radioactivity was significantly reduced in heart, liver, lungs, spleen, and kidneys. The tumor-to-muscle ratio gradually increased and peaked after 240 h (**Fig. 4K**). Thus, 9MW2821 had high specificity for nectin-4 and a long duration of tumor suppression.

Antitumor efficacy of 9MW2821 in multiple CDX

We evaluated the antitumor activities of 9MW2821 and EV in a variety of CDX models that covered multiple conditions.

In NCI-H322 (**Fig. 5A**) and MDA-MB-468 (**Fig. 5B**) xenografts, 9MW2821 showed antitumor efficacy superior to EV after treatment

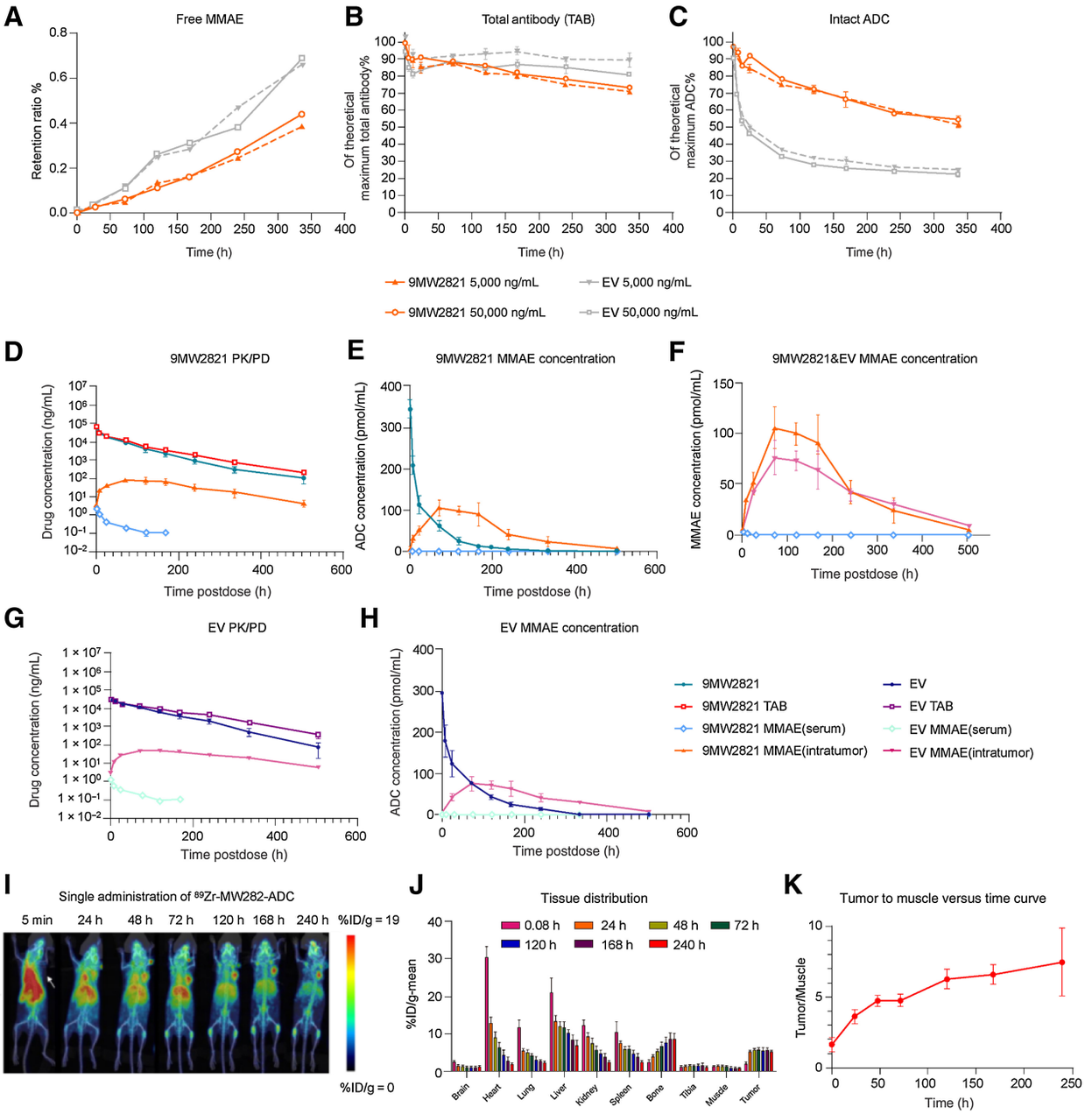

Figure 4.

Pharmacokinetic profile of 9MW2821. **A–C,** *In vitro* serum stability of 9MW2821 and EV in monkey serum at 37°C from 0 to 14 days. **A,** Release rate of free MMAE of two ADC measured by LC/MS-MS. The LC/MS-MS method was validated for accuracy. **B, C,** Total antibodies and intact ADC were quantified by ELISA. The data are mean values for double measurements. **D–H,** Pharmacokinetic profiles of 9MW2821 and EV in MDA-MB-468 tumor-bearing mice ($n = 54$, each group). Six animals were included in each blood collection point. **D** and **G,** We compared the PK profile of 9MW2821 with EV for free MMAE in serum, intact ADC, total antibodies, and MMAE intra-tumors. **E** and **H,** We compared the ADC in mole numbers of free MMAE in serum, intact ADC in serum, and MMAE intratumors. **F,** We compared the free MMAE in serum and MMAE intratumors in one picture. **I–K,** Tissue distribution of 9MW2821 in tumor-bearing mice ($n = 6$). MIP images of PET/CT scanning of MDA-MB-468 tumor-bearing mice after a single intravenous administration of ^{89}Zr-9MW2821 at different timepoints. The average tumor-to-muscle ratio showed a rising trend, reaching a peak value of 7.48 at 240 h postdose. The absorption of radioactivity was significantly less in the heart, liver, lung, spleen, and kidney.

with the same doses. A single administration of 3 mg/kg and 10 mg/kg 9MW2821 led to TGI of 83% and 134%, respectively, which was greater than the 64% and 123% in the EV group ($n = 8$, $p < 0.05$). Furthermore, with a similar treatment protocol (single-dose administration at 3 mg/kg and 10 mg/kg) in the MDA-MB-468 xenograft, TGI of 64% and 111% was achieved with 9MW2821. This result was also better than 37%, 72% for EV ($n = 8$, $P < 0.05$). Furthermore, the effective doses of 9MW2821 were 1 mg/kg in NCI-H322 cells and 3 mg/kg in MDA-MB-468 cells, which were lower dose concentrations than the doses of EV in these two models.

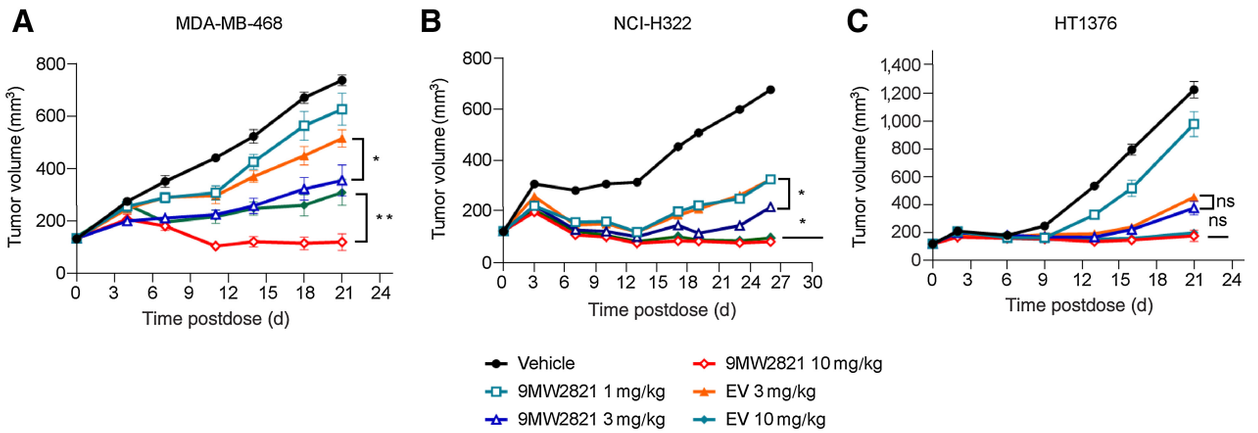

Figure 5.

Antitumor efficacy of 9MW2821 in CDXs. **A–C,** TGI evaluated in MDA-MB-468, NCI-H322M, HT1376 xenograft models. Xenograft mice ($n = 8$) were intravenously treated with 1, 3, or 10 mg/kg 9MW2821 or EV at 3 mg/kg or 10 mg/kg for one injection. All treatments were initiated on the day when the average tumor volume reached 100 to 150 mm^3. The tumor inhibition rates are mean values of eight animals.

In the HT1376 xenograft, 9MW2821 exhibited anti–bladder tumor activity equal to EV. (**Fig. 5C**). The HT1376 xenograft exhibited TGI of 77% and 95% after treatment with 3 mg/kg and 10 mg/kg 9MW2821, which was not significantly different from the 70% and 93% inhibition by EV at the same doses. ($n = 8$, $P > 0.05$). The high antitumor responses in both treatment groups were akin to the high efficacy of EV toward urothelial carcinoma in clinical use.

In all models, treatments were well tolerated, with minimal body weight loss (Supplementary Fig. S10) and no adverse effects observed.

Antitumor efficacy of 9MW2821 in PDX

On the basis of the encouraging antitumor efficacy of 9MW2821 in CDX models, we next evaluated PDX that covered multiple indications. (**Fig. 6A–G**)

In the urothelial carcinoma (BL3578, H-score 137), triple-negative breast cancer (BR9457, H-score 235), non–small cell lung cancer (NSCLC; LU3073, H-score 210), and cervical carcinoma models (CV13641, H-score 249), treatment with 9MW2821 led to tumor stasis. Furthermore, in the LU3073 model, 9MW2821 showed antitumor activity greater than EV. The 9MW2821 conjugate produced rapid tumor regression and long-lasting tumor suppression in nectin-4 high-expression PDX models.

The considerable antitumor efficacies were associated with high nectin-4 expression. However, tumors with medium or low nectin-4 expression were also susceptible to 9MW2821. In BR9479 (H-score: 157) xenografts, treatment with 9MW2821 at 3 mg/kg led to TGI of 97%. In BR1282 (H-score: 63) or BR1458 (H-score: 7), 9MW2821 also showed high or partial effect, resulting in 49% and 51% TGI, respectively. We analyzed FFPE samples from BR1282 after treatment of 9MW2821 and found that the H-score reduced to 0. (Supplementary Fig. S11) Besides nectin-4 expression, penetration into solid tumors is another key factor that affects drug efficacy (23). In CV13641, LU3073, or BR9457, 9MW2821 showed comparable activity between large and small tumors, which indicated good tumor penetration of 9MW2821.

In all models, treatments were well tolerated, with minimal body weight loss (Supplementary Fig. S12) and no adverse effects were observed.

Safety study of 9MW2821

We comprehensively evaluated the safety profile of 9MW2821 administered to cynomolgus monkeys. After repeated doses of 9MW2821 (1, 3, and 6 mg/kg, QW × 5) or MW282 mAb (6 mg/kg, QW × 5) for 9 weeks, major toxicities, such as skin redness, fever, and dandruff, were observed in the 6 mg/kg ADC group, and little dandruff was observed in the 3 mg/kg group. The hematotoxicity and myelotoxicity observed were directly related to the dosage administered and were reversible. These toxicities primarily manifested as a decrease in the erythrocyte count, as well as a temporary decrease followed by an increase in reticulocytes and white blood cells (Supplementary Table S13–S16). No obvious abnormalities were observed in food consumption and body weight (Supplementary Fig. S13), and there were no toxicologically significant changes in cardiovascular, respiratory, or neurologic properties. In cynomolgus monkeys, the highest dose that did not cause severe toxicity was 6 mg/kg.

We incorporated toxicokinetic studies into the safety assessment to determine the exposure levels of 9MW2821, total antibody, and free MMAE at 1, 3, and 6 mg/kg during the first and fourth dose cycles. The serum concentrations of 9MW2821 and total antibody in each group rapidly peaked after administration, whereas MMAE in most peaked at 8 to 48 h postdose. Exposure to 9MW2821, total antibody, or MMAE increased proportionally with the dose, and there was no obvious accumulation of the three after repeated doses. The corresponding exposures to 9MW2821, total antibody, and free MMAE on day 22 are summarized in Supplementary Table S12.

Discussion

The 9MW2821 conjugate is the first site-specific nectin-4 ADC; 9MW2821 shares the same cleavable linker and toxin as EV. The 9MW2821 conjugate had excellent tumor inhibitory effects in animal models of many cancer types, such as lung, breast, cervical, and bladder cancers. In some xenografts, the antitumor activity of 9MW2821 was superior to that of EV at the same dose. In addition, promising antitumor efficacies were observed in urothelial carcinoma, triple-negative breast cancer, NSCLC, and cervical carcinoma PDX models with various levels of nectin-4 expression. The repeat-dose administration of 9MW2821 at 3 mg/kg produced a

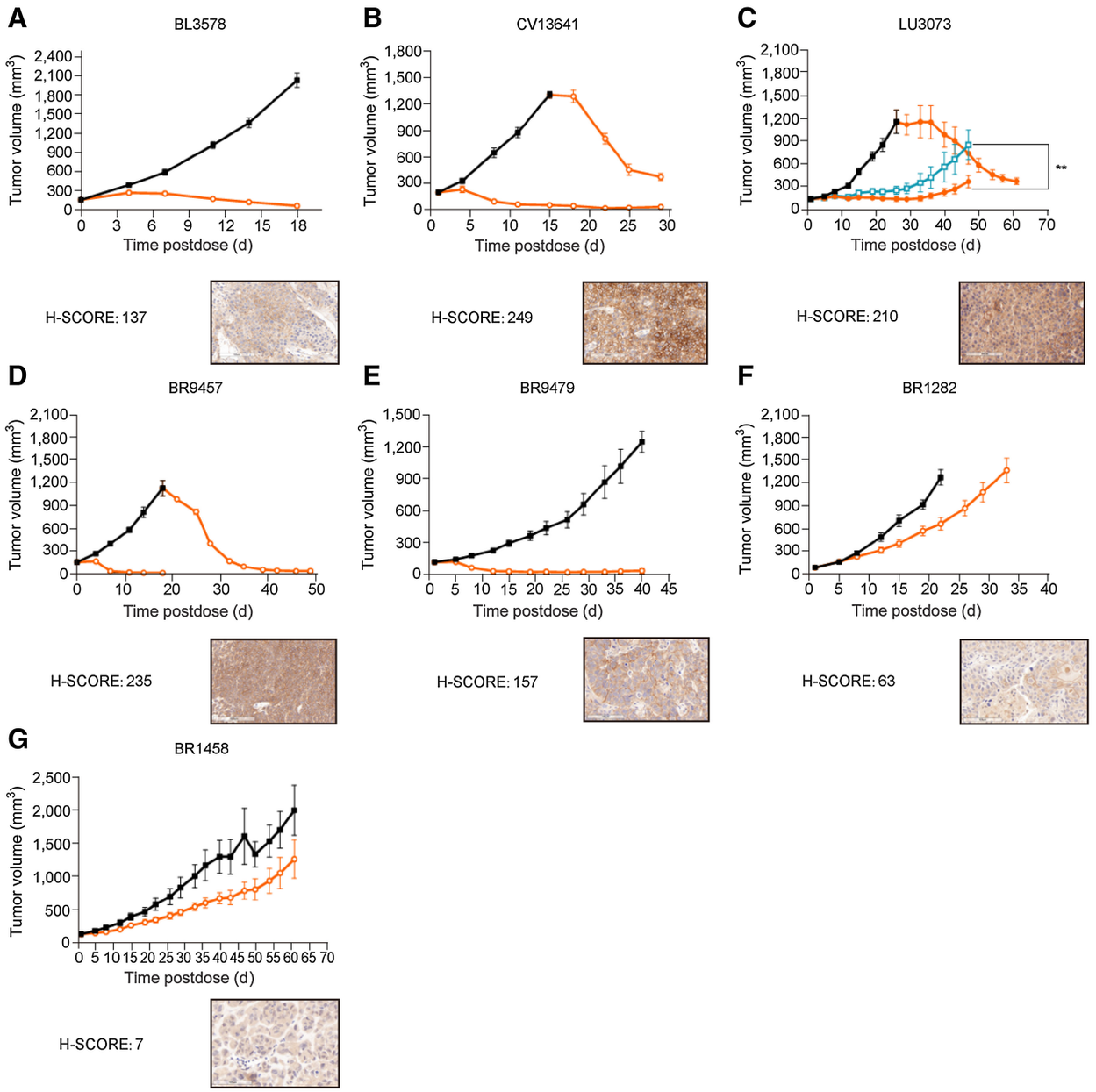

Figure 6.

Antitumor efficacy of 9MW2821 in PDX. Seven typical PDX models were evaluated for antitumor efficacy: bladder cancer (BL3578), cervical cancer (CV13641), lung cancer (LU3073), and four triple-negative breast cancers (BR9457, BR9479, BR1282, and BR1458). **A,** BL3578 xenograft mice were intravenously treated with three injections of 3 mg/kg 9MW2821 once a week. **B,** CV13641 xenograft mice were intravenously treated with three injections of 3 mg/kg 9MW2821 weekly. The vehicle group was administered in three repeat doses ($n = 8$, 3 mg/kg, weekly) after the tumor volumes reached 100 mm^3. **C,** CV13641 xenograft mice were intravenously treated with 3 mg/kg 9MW2821 and EV respectively once a week for three injections. Then the vehicle group was repeat dosed ($n = 8$, 3 mg/kg, weekly) after the tumor volumes reached 100 mm^3. **D–G,** Four typical triple-negative breast cancers with different nectin-4 expression were also treated with three injections of 3 mg/kg 9MW2821 weekly. For BR9457, the vehicle group was also administered three repeat doses ($n = 8$, 3 mg/kg, weekly) after the tumor volumes reached 100 mm^3.

complete response in tumors with high nectin-4 expression. In triple-negative breast cancer PDX models with medium or low antigen expression (H-score 157, 63, or 7), 9MW2821 also had a strong antitumor effect, which indicated that 9MW2821 eradicated heterogenous nectin-4–expressing tumors.

In addition to these desirable properties, 9MW2821 had a favorable safety profile in monkeys. In humans during EV treatment, 51.4% of patients experienced grade 3 or higher adverse events. These treatment-related adverse events frequently result in dose reduction and/or treatment discontinuation (25). Similarly, EV elicited severe adverse

reactions in our preclinical evaluation. Approximately 30% of the monkeys died after receiving EV at 6 mg/kg, and deaths were reported as early as study day 11. Deaths were attributed to severe skin lesions, lethargy, bone marrow toxicity, gastrointestinal tract toxicity, and liver toxicity (43). Conversely, in our general toxicity studies, 9MW2821 produced milder adverse reactions and demonstrated a higher dose at which toxicity was not severe (6 mg/kg); compared with EV, these properties of 9MW2821 suggested better tolerance and an expectation of better patient compliance in clinical use.

Delivery of sufficient payload to the intracellular target of the tumor and avoidance of off-target cytotoxicity are major challenges to clinical application of ADC. We employed many factors to ensure the efficiency and specificity of 9MW2821 drug delivery. First, we designed and developed a novel thioether linker (IDconnect) to produce a site-specific ADC. IDconnect was based on a novel maleimide scaffold with a 4-mercapto-benzoyl-morpholine leaving group in the 3- and 4-positions; this group was designed to improve water solubility and decrease nucleophilicity of the conventional thiophenol group (Supplementary Fig. S1A; ref. 34). This linker-payload complex would facilitate site-specific conjugation without introduction of cysteine mutations or nonnatural amino acids. Biochemical characterization showed that 9MW2821 maintained high purity and a homogenous DAR of 4. This special conjugation also preserved the original properties of the parental antibody, such as binding affinity, antibody-dependent cell-mediated cytotoxicity, and affinity to Fcγ and FcRn. Conventional stochastic conjugation methods generate EV that contains a mixture of molecules with varying DAR and sites of conjugation (Supplementary Fig. S3; refs. 44, 45). The heterogeneous mixtures can have significant differences in binding affinity, stability, and pharmacokinetics and pharmacodynamics profiles, which leads to variability in toxicity and efficacy in patients (46, 47). A site-specific and highly homogenous ADC with a DAR of 4 can properly balance drug delivery and pharmacokinetic stability. In addition, the 3,5-difluorophenyl moiety in our design accelerated the complete hydrolysis of the maleimide, which prevented deconjugation by the retro-Michael reaction, thereby stabilizing the antibody conjugate (34, 48, 49). Although N-aryl maleimide is commonly used to accelerate in situ maleimide hydrolysis to make an ADC stable at physiological pH, this linkage-complex can be cleaved quantitatively in a mildly acidic environment. By introducing the 3,5-difluorophenyl group, we avoided this undesirable drug release and further enhanced ADC stability (28, 49). We also found that this linker system used in 9MW2821 enhanced the internalization rate, which, in turn, improved intratumoral exposure to MMAE. Thus, 9MW2821 not only showed great efficacy toward tumors with high nectin-4 expression, but also 9MW2821 exerted excellent cell killing of tumors that had medium or low nectin-4 antigen expression.

To prevent the off-target toxicities that have resulted from deconjugation of payloads or linker cleavage associated with conventional ADC, we used a thioether bridge linker that was highly stable in the circulation. We observed improved stability *in vivo* as evidenced by the small difference between the intact ADC and total antibody pharmacokinetic profiles. Our preclinical safety studies of 9MW2821 conducted in nonhuman primates with doses up to 6 mg/kg for five doses showed mostly mild on-target epithelial toxicities (such as skin redness and dandruff) that were fully reversible. Toxicokinetic studies showed that 9MW2821 had lower systemic ADC exposure ($AUC_{0\text{-}t}$ = 1,050 h/μg/mL for 9MW2821 3 mpk vs. $AUC_{0\text{-}t}$ = 2,530 h/μg/mL for EV 3 mpk, ref. 43). This lower exposure may be another explanation for the milder toxicity of 9MW2821.

In summary, 9MW2821 exhibited many desirable properties as a novel nectin-4-targeting ADC: a homogeneous DAR, tumor-specific accumulation, effective bystander effect, excellent efficacy in xenograft models, and acceptable safety margin in monkeys. These results warrant further investigation of this novel ADC in patients with solid tumors, and a phase I/II clinical trial (NCT05216965 and NCT05773937) of 9MW2821 is ongoing.

Authors' Disclosures

No disclosures were reported.

Authors' Contributions

W. Zhou: Conceptualization, formal analysis, supervision, investigation, methodology, writing–original draft, writing–review, and editing. **P. Fang:** Data curation, formal analysis, supervision, investigation, methodology, and writing–original draft. **D. Yu:** Data curation, formal analysis, supervision, investigation, methodology, and writing–original draft. **H. Ren:** Supervision, investigation, and methodology. **M. You:** Supervision, investigation, and methodology. **L. Yin:** Supervision, investigation, and methodology. **F. Mei:** Supervision, investigation, and methodology. **H. Zhu:** Investigation and methodology. **Z. Wang:** Investigation, and methodology. **H. Xu:** Investigation and methodology. **Y. Cao:** Data curation, investigation, visualization, and methodology. **X. Sun:** Data curation, investigation, and methodology. **X. Xu:** Data curation, investigation, and visualization, methodology. **J. Bi:** Data curation, investigation, visualization, and methodology. **J. Wang:** Data curation, investigation, visualization, and methodology. **L. Ma:** Conceptualization, investigation, and methodology. **X. Wang:** Conceptualization, investigation, and methodology. **L. Chen:** Investigation and visualization. **Y. Zhang:** Investigation and visualization. **X. Cen:** Writing–original draft. **X. Zhu:** Data curation, investigation, and methodology. **L. Lou:** Data curation, investigation, and methodology. **D. Liu:** Resources and supervision. **X. Tan:** Conceptualization, formal analysis, supervision, and investigation. **J. Yang:** Resources, formal analysis, supervision, investigation, writing–review, and editing. **T. Meng:** Conceptualization, supervision, investigation, methodology, writing–original draft, writing–review, and editing. **J. Shen:** Conceptualization, resources, supervision, investigation, and methodology.

Acknowledgments

The preclinical studies received funding from Mabwell (Shanghai) Bioscience Co., Ltd. The authors thank Puremab Biotech for their support during the early stages of antibody discovery and generation. Beijing Kohnoor Science & Technology Inc. contributed to cell line construction and antibody humanization. Patient-derived xenograft studies were conducted with the assistance of Crown Bioscience Inc. General toxicology studies were carried out by CDSER, Shanghai Institute of Materia Medica, while tissue distribution studies were conducted by MITRO Biotech, Inc. Shanghai Haoyuan Chemexpress Inc. provided support for linker-payload synthesis. Huiting Yue and Xiaohong Zhu from Jiangsu Mabwell Health Pharmaceutical R&D Co. assisted with data collection and review. Yiran Tao from West China-California Research Center for Predictive Intervention Medicine, West China Hospital, Sichuan University contributed to antibody-dependent cell-mediated cytotoxicities measured through a cell-based reporter-gene assay. English language editing and review services were provided by AiMi Academic Services (www.aimieditor.com).

Note

Supplementary data for this article are available at Molecular Cancer Therapeutics Online (http://mct.aacrjournals.org/).

Received November 15, 2022; revised March 31, 2023; accepted May 12, 2023; published first May 17, 2023.

References

1. Samanta D, Almo SC. Nectin family of cell-adhesion molecules: structural and molecular aspects of function and specificity. Cell Mol Life Sci 2015;72:645–58.
2. Bouleftour W, Guillot A, Magne N. The anti-nectin 4: a promising tumor cells target. a systematic review. Mol Cancer Ther 2022;21:493–501.

3. Reymond N, Fabre S, Lecocq E, Adelaide J, Dubreuil P, Lopez M. Nectin4/PRR4, a new afadin-associated member of the nectin family that trans-interacts with nectin1/PRR1 through V domain interaction. J Biol Chem 2001;276:43205–15.
4. Noyce RS, Bondre DG, Ha MN, Lin L-T, Sisson G, Tsao M-S, et al. Tumor cell marker PVRL4 (nectin 4) is an epithelial cell receptor for measles virus. PLoS Pathog 2011;7:e1002240.
5. Mühlebach MD, Mateo M, Sinn PL, Prüfer S, Uhlig KM, Leonard VH, et al. Adherens junction protein nectin-4 is the epithelial receptor for measles virus. Nature 2011;480:530–3.
6. Takano A, Ishikawa N, Nishino R, Masuda K, Yasui W, Inai K, et al. Identification of nectin-4 oncoprotein as a diagnostic and therapeutic target for lung cancer. Cancer Res 2009;69:6694–703.
7. Sethy C, Goutam K, Nayak D, Pradhan R, Molla S, Chatterjee S, et al. Clinical significance of a pvrl 4 encoded gene Nectin-4 in metastasis and angiogenesis for tumor relapse. J Cancer Res Clin Oncol 2020;146:245–59.
8. Xu G, Ma J, Sheng Z, Lv Y, Liu W, Yao Q, et al. Expression and clinical significance of nectin-4 in hepatocellular carcinoma. Onco Targets Ther 2016;9:183–90.
9. Derycke MS, Pambuccian SE, Gilks CB, Kalloger SE, Ghidouche A, Lopez M, et al. Nectin 4 overexpression in ovarian cancer tissues and serum: potential role as a serum biomarker. Am J Clin Pathol 2010;134:835–45.
10. Heath EI, Rosenberg JE. The biology and rationale of targeting nectin-4 in urothelial carcinoma. Nat Rev Urol 2021;18:93–103.
11. Miyoshi J, Takai Y. Nectin and nectin-like molecules: biology and pathology. Am J Nephrol 2007;27:590–604.
12. Zhang Y, Chen P, Yin W, Ji Y, Shen Q, Ni Q. Nectin-4 promotes gastric cancer progression via the PI3K/AKT signaling pathway. Hum Pathol 2018;72:107–16.
13. Siddharth S, Goutam K, Das S, Nayak A, Nayak D, Sethy C, et al. Nectin-4 is a breast cancer stem cell marker that induces WNT/beta-catenin signaling via Pi3k/Akt axis. Int J Biochem Cell Biol 2017;89:85–94.
14. Kedashiro S, Sugiura A, Mizutani K, Takai Y. Nectin-4 cis-interacts with ErbB2 and its trastuzumab-resistant splice variants, enhancing their activation and DNA synthesis. Sci Rep 2019;9:1–15.
15. Siddharth S, Nayak A, Das S, Nayak D, Panda J, Wyatt MD, et al. The soluble nectin-4 ecto-domain promotes breast cancer induced angiogenesis via endothelial Integrin-β4. Int J Biochem Cell Biol 2018;102:151–60.
16. Reches A, Ophir Y, Stein N, Kol I, Isaacson B, Amikam YC, et al. Nectin4 is a novel TIGIT ligand which combines checkpoint inhibition and tumor specificity. J Immunother Cancer 2020;8:e000266.
17. Diamantis N, Banerji U. Antibody-drug conjugates—an emerging class of cancer treatment. Br J Cancer 2016;114:362–7.
18. Casi G, Neri D. Antibody–drug conjugates: basic concepts, examples and future perspectives. J Control Release 2012;161:422–8.
19. Kim SB, Wildiers H, Krop IE, Smitt M, Yu R, Lysbet de Haas S, et al. Relationship between tumor biomarkers and efficacy in TH3RESA, a phase III study of trastuzumab emtansine (T-DM1) vs. treatment of physician's choice in previously treated HER2-positive advanced breast cancer. Int J Cancer 2016;139:2336–42.
20. Bussing D, Sharma S, Li Z, Meyer LF, Shah DK. Quantitative evaluation of the effect of antigen expression level on antibody–drug conjugate exposure in solid tumor. The AAPS Journal 2021;23:56.
21. Challita-Eid PM, Satpayev D, Yang P, An Z, Morrison K, Shostak Y, et al. Enfortumab vedotin antibody-drug conjugate targeting nectin-4 is a highly potent therapeutic agent in multiple preclinical cancer models. Cancer Res 2016;76:3003–13.
22. FDA approves new type of therapy to treat advanced urothelial cancer. Available from https://www.fda.gov/news-events/press-announcements/fda-approves-new-type-therapy-treat-advanced-urothelial-cancer.
23. Rigby M, Bennett G, Chen L, Mudd GE, Harrison H, Beswick PJ, et al. BT8009; a nectin-4 targeting Bicycle toxin conjugate for treatment of solid tumors. Mol Cancer Ther 2022;21:1747–56.
24. McKean M, Baldini C, Verlingue L, Doger B, Falchook G, Italiano A, et al. Abstract CT025: BT8009–100 phase I/II study of novel bi-cyclic peptide and MMAE conjugate BT8009 in patients with advanced malignancies associated with nectin-4 expression. Cancer Res 2022;82(10 suppl):CT025.
25. Powles T, Rosenberg JE, Sonpavde GP, Loriot Y, Duran I, Lee JL, et al. Enfortumab vedotin in previously treated advanced urothelial carcinoma. N Engl J Med 2021;384:1125–35.
26. Ren H, Zhu J, Lin J, Wang L, Xu X, Deng X, et al. Mabwell Shanghai Bioscience Co Ltd. Antibody Against Nectin-4 And Application Thereof. Patent WO2021213434A1.
27. Athanassiadou AM, Patsouris E, Tsipis A, Gonidi M, Athanassiadou P. The significance of survivin and nectin-4 expression in the prognosis of breast carcinoma. Folia Histochem Cytobiol 2011;49:26–33.
28. Shen J, Meng T, Ma L, Wang X, Peng H, Zhang Y, et al. Mabwell Shanghai Bioscience Co Ltd. Di-Substituted Maleic Amide Linker for Antibody Drug Conjugating and Preparation method and use thereof. Patent US201716464211A.
29. Zhou W, Zhu H, Wang Z, Xu H, Tan X, et al. Mabwell Shanghai Bioscience Co Ltd. Preparation Method for Bis-Substituted Bridging Antibody-Drug Conjugate. Patent WO2022068898A1.
30. Hsieh YT, Aggarwal P, Cirelli D, Gu L, Surowy T, Mozier NM. Characterization of FcγRIIIA effector cells used in in vitro ADCC bioassay: comparison of primary NK cells with engineered NK-92 and Jurkat T cells. J Immunol Methods 2017;441:56–66.
31. England CG, Ehlerding EB, Hernandez R, Rekoske BT, Graves SA, Sun H, et al. Preclinical pharmacokinetics and biodistribution studies of 89Zr-labeled pembrolizumab for human dosimetry estimation. J Nucl Med 2016;58:162–8.
32. Abou DS, Ku T, Smith-Jones PM. In vivo biodistribution and accumulation of 89Zr in mice. Nucl Med Biol 2011;38:675–81.
33. Zheleznyak A, Ikotun OF, Dimitry J, Frazier WA, Lapi SE. Imaging of CD47 expression in xenograft and allograft tumor models. Mol Imaging 2013;12:525–34.
34. Schumacher FF, Nunes JP, Maruani A, Chudasama V, Smith ME, Chester KA, et al. Next generation maleimides enable the controlled assembly of antibody-drug conjugates via native disulfide bond bridging. Org Biomol Chem 2014;12:7261–9.
35. An D, Han N, Li J, Li M, Yang C, Yang H, et al. Newbio Therapeutics, Inc. Tridentate connexon and use thereof. patent US10960082B2.
36. Han N, An D, Zeng D, Wang B, Yang H, Li J, et al. Newbio Therapeutics Inc. Trimaleimide linkers and uses thereof. patents US10314922B2.
37. Han N, An D, Zeng D, Wang B, Li H, Chen H, et al. Shanghai New Concept Biomedical Tech Co. Ltd. Oxadiazole connexons and application thereof. patents US11241503B2.
38. Guo M, Li H, Li H, Zheng X, Jia Z, Wang W, et al. Tanning Suzhou Biopharmacy Co. Ltd. Bromomethylpyrazine-based drug conjugate and ADC. patent CN114106088A.
39. Kovtun YV, Audette CA, Ye Y, Xie H, Ruberti MF, Phinney SJ, et al. Antibody-drug conjugates designed to eradicate tumors with homogeneous and heterogeneous expression of the target antigen. Cancer Res 2006;66:3214–21.
40. Lyon RP, Setter JR, Bovee TD, Doronina SO, Hunter JH, Anderson ME, et al. Self-hydrolyzing maleimides improve the stability and pharmacological properties of antibody-drug conjugates. Nat Biotechnol 2014;32:1059–62.
41. Tumey LN, Charati M, He T, Sousa E, Ma D, Han X, et al. Mild method for succinimide hydrolysis on ADCs: impact on ADC potency, stability, exposure, and efficacy. Bioconjug Chem 2014;25:1871–80.
42. Wei C, Zhang G, Clark T, Barletta F, Tumey LN, Rago B, et al. Where did the linker-payload go? A quantitative investigation on the destination of the released linker-payload from an antibody-drug conjugate with a maleimide linker in plasma. Anal Chem 2016;88:4979–86.
43. Enfortumab vedotin multi-disciplinary review and evaluation. Available from: https://www.accessdata.fda.gov/drugsatfda_docs/nda/2019/761137Orig1s000MultiDisciplineR.pdf.
44. Chen T, Chen Y, Stella C, Medley CD, Gruenhagen JA, Zhang K. Antibody-drug conjugate characterization by chromatographic and electrophoretic techniques. J Chromatogr B 2016;1032:39–50.
45. Chen T-H, Yang Y, Zhang Z, Fu C, Zhang Q, Williams JD, et al. Native reversed-phase liquid chromatography: a technique for LCMS of intact antibody–drug conjugates. Anal Chem 2019;91:2805–12.
46. Junutula JR, Raab H, Clark S, Bhakta S, Leipold DD, Weir S, et al. Site-specific conjugation of a cytotoxic drug to an antibody improves the therapeutic index. Nat Biotechnol 2008;26:925–32.
47. Panowski S, Bhakta S, Raab H, Polakis P, Junutula JR. Site-specific antibody drug conjugates for cancer therapy. mAbs. 2014;6:34–45.
48. Nunes JP, Morais M, Vassileva V, Robinson E, Rajkumar VS, Smith ME, et al. Functional native disulfide bridging enables delivery of a potent, stable and targeted antibody–drug conjugate (ADC). Chem Commun 2015;51:10624–7.
49. Christie RJ, Fleming R, Bezabeh B, Woods R, Mao S, Harper J, et al. Stabilization of cysteine-linked antibody drug conjugates with N-aryl maleimides. J Control Release 2015;220:660–70.